Journal of Electronics, Electromedical Engineering, and Medical Informatics
Homepage: jeeemi.org; Vol. 7, No. 4, October 2025, pp: 1028-1044 e-ISSN: 2656-8632

RESEARCH ARTICLE

OPEN ACCESS

A Reproducible Workflow for Liver Volume Segmentation and 3D Model Generation Using Open-Source Tools

Badreddine Labakoum[1,2], Hamid El Malali [1], Amr Farhan[1,2], Azeddine Mouhsen [1], and Aissam Lyazidi [2]

[1] Energy-Materials-Instrumentation and Telecom Laboratory (EMIT), Faculty of Science and Technology, University Hassan 1st, Settat, Morocco
[2] Sciences and Engineering of Biomedicals, Biophysics and Health Laboratory, Higher Institute of Health Sciences (ISSS), University Hassan 1st, Settat, Morocco

Corresponding author: Badreddine Labakoum. (e-mail: b.labakoum@uhp.ac.ma), **Author(s) Email**: Hamid El Malali (e-mail: hamid.elmalali@uhp.ac.ma, Amr Farhan (e-mail: a.farhan@uhp.ac.ma, Azeddine Mouhsen (e-mail: azmouhsen@gmail.com), Aissam Lyazidi (e-mail: aissam.lyazidi@uhp.ac.ma))

Abstract **Complex liver resections related to hepatic tumors represent a major surgical challenge that requires precise preoperative planning supported by reliable three-dimensional (3D) anatomical models. In this context, accurate volumetric segmentation of the liver is a critical prerequisite to ensure the fidelity of printed models and to optimize surgical decision-making. This study compares different segmentation techniques integrated into open-source software to identify the most suitable approach for clinical application in resource-limited settings. Three semi-automatic methods, region growing, thresholding, and contour interpolation, were tested using the 3D Slicer platform and compared with a proprietary automatic method (Hepatic VCAR, GE Healthcare) and a manual segmentation reference, considered the gold standard. Ten anonymized abdominal CT volumes from the Medical Segmentation Decathlon dataset, encompassing various hepatic pathologies, were used to assess and compare the performance of each technique. Evaluation metrics included the Dice similarity coefficient (Dice), Hausdorff distance (HD), root mean square error (RMS), standard deviation (SD), and colorimetric surface discrepancy maps, enabling both quantitative and qualitative analysis of segmentation accuracy. Among the tested methods, the semi-automatic region growing approach demonstrated the highest agreement with manual segmentation (Dice = 0.935 ± 0.013; HD = 4.32 ± 0.48 mm), surpassing both other semi-automatic techniques and the automatic proprietary method. These results suggest that the region growing method implemented in 3D Slicer offers a reliable, accurate, and reproducible workflow for generating 3D liver models, particularly in surgical environments with limited access to advanced commercial solutions. The proposed methodology can potentially improve surgical planning, enhance training through realistic patient-specific models, and facilitate broader adoption of 3D printing in hepatobiliary surgery worldwide.**

Keywords **Hepatic resection; Surgical simulation; 3D modelling; Image segmentation; Preoperative planning**.

I. Introduction

Hepatocellular carcinoma (HCC), a major form of liver cancer, is among the six most frequently diagnosed cancers globally and stands as the third most common cause of cancer-related deaths. Chronic hepatitis B and C infections are the main contributing factors[1][2][3]. Hepatic resection remains the standard and effective curative treatment for the disease[4]. However, the localization and precision of the ablation of the parts to be removed are extremely complex because the liver is one of the most vascularized organs. Indeed, the resection of tumor areas must be performed in such a way as to leave no chance for their recurrence, while preserving an adequate portion[5][6]. In this context, the importance of simulating the operation on a 3D model with the same physical characteristics and dimensions prepared in advance comes into play[7][8][9]. Indeed, surgical simulation plays a crucial role in the effective planning and precision of surgical procedures, with the main objective of minimizing the risks associated with human errors[10][11][12][13]. In modern medicine, simulation constitutes a practical virtual reality that allows for the training of new surgeons as well as the simulation of a

Manuscript received June 8, 2025; Revised August 20, 2025; Accepted August 30, 2025; date of publication September 1, 2025
Digital Object Identifier (**DOI**): https://doi.org/10.35882/jeeemi.v7i4.1086

procedure before performing it on the patient, especially when it involves a complex or unusual procedure such as the removal of cancerous parts of an organ without affecting the surrounding healthy vital tissues[14][15][16][17]. These objectives can only be achieved if the prepared phantoms accurately reflect the reality of the organ to be simulated[18][19][20]. In general, the preparation of 3D phantoms relies on the segmentation of the studied organ from medical images such as CT or MRI scans[21][22]. Indeed, segmentation is the operation that involves partitioning the image into a set of regions sharing the same properties (texture, grayscale level, color...)[23][24]. The accuracy of the 3D model is related to the performance of the segmentation method used[25][26][27].

In resource-limited clinical settings, healthcare professionals face several concrete challenges: lack of high-performance workstations (especially without GPUs), time constraints, high costs of proprietary software, and limited availability of trained personnel in advanced imaging. These constraints significantly hinder the adoption of automated or commercial solutions, highlighting the need for accessible and reliable open-source alternatives. Tools like 3D Slicer enable local execution of semi-automatic segmentation with user control, while remaining compatible with standard computing infrastructure. This approach effectively compromises accuracy, reproducibility, and accessibility in constrained environments.

In clinical environments with limited resources, such as public hospitals or regional centers, open-source software, particularly platforms like 3D Slicer or ITK-SNAP, provides a reliable, accessible, and economically viable alternative for volumetric liver segmentation. Unlike fully automated approaches based on artificial intelligence, which require massive annotated databases, advanced hardware resources (notably GPUs), and specific algorithmic expertise [28][29][30], the semi-automatic methods integrated into these environments (region growing, thresholding, contour interpolation) allow for an effective compromise between precision, flexibility, and ease of use [31][32]. In addition to operating locally, which enhances the protection of sensitive data, these tools offer clinicians the ability to manually intervene on the segmented contours, an essential asset for addressing complex clinical situations, such as multifocal liver tumors or poor-quality images [33][34]. Moreover, the open-source ecosystem benefits from active support from the scientific community, with abundant documentation, regular updates, and robust validation in specialized literature [30]. These characteristics ensure the results' reproducibility, transparency, and reliability, fundamental conditions for secure integration into clinical protocols. As a result, these solutions prove to be particularly relevant for personalized surgical planning assisted by 3D models, providing healthcare professionals with, practical tools without compromising the quality or safety of care, even in a constrained economic context.

Although several recent works have demonstrated the growing interest in 3D liver segmentation using open-source platforms such as 3D Slicer, the majority of these studies focus either on specific technical extensions, such as hepatic and vascular segmentation in the R Vessel X project [35][36], or on the integration of advanced artificial intelligence models such as 3D U Net networks or the Segment Anything (SAM) model via extensions like FastSAM 3DSlicer [37][38]. Although effective in terms of algorithmic precision, these approaches present several major limitations in a clinical context with limited resources: they generally require heavy computing infrastructure (GPU, cloud), massive annotated databases, and advanced technical expertise. Other, more applied works focus on specific structures such as the bile ducts or reconstructions from ultrasound images, without offering a systematic comparison between different segmentation methods usable in a standardized preoperative workflow. However, no standardized comparative study has systematically evaluated these semi-automatic tools under real clinical constraints[39][40][41].

Faced with this gap, the choice to resort to semi-automatic methods is based on their ease of integration into real clinical environments, robustness against heterogeneous data, and ability to combine user guidance with effective algorithmic processing. Preliminary results from the literature and clinical experimentation indicate that some of these methods, particularly those natively integrated into 3D Slicer, achieve accuracy comparable to proprietary solutions while offering crucial interactive control in complex cases. However, in the absence of validated, accessible comparative studies in constrained clinical environments, it becomes necessary to evaluate these tools using a standardized and clinically realistic approach.

To provide a precise methodological framework, this study is structured around the following research questions:

1. Can semi-automatic region growing achieve a geometric accuracy comparable to manual segmentation?
2. Which native segmentation method in 3D Slicer offers the best compromise between accuracy, reproducibility, and clinical usability?

Manuscript received June 8, 2025; Revised August 20, 2025; Accepted August 30, 2025; date of publication September 1, 2025
Digital Object Identifier (**DOI**): https://doi.org/10.35882/jeeemi.v7i4.1086

3. To what extent can open-source segmentation methods be used to generate 3D-printable liver models for surgical planning in patients with hepatic metastases?

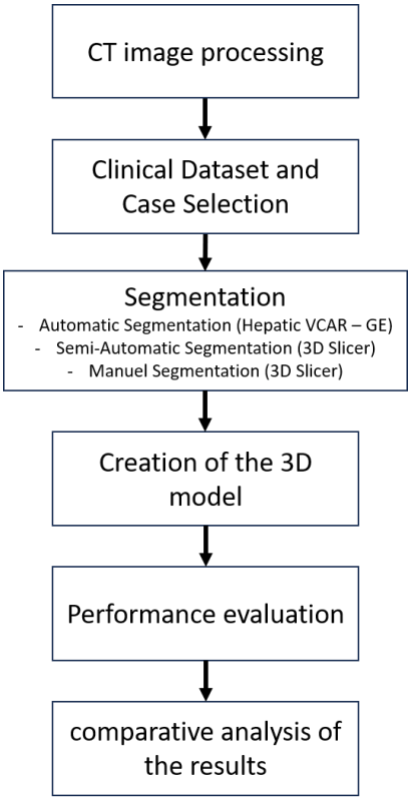

Fig. 1. Diagram of the experimental

Accordingly, the main objective of this work is to propose a reproducible, low-cost, and clinically applicable workflow for liver segmentation and 3D model generation using only native semi-automatic tools available in 3D Slicer, without relying on artificial intelligence or commercial software. Based on contrast-enhanced abdominal CT data from patients with liver metastases. Three approaches were explored: automatic segmentation (Hepatic VCAR), semi-automatic segmentation (region growing, thresholding, and contour interpolation) using the open-source software 3D Slicer, and manual segmentation, which served as a reference. The study aims to identify the method offering the best compromise between precision, result stability, and operational efficiency, particularly in clinical contexts with limited resources. The main contributions of this study are as follows: (1) a systematic comparison of native 3D Slicer semi-automatic segmentation methods applied to liver CT data; (2) the integration of this workflow into a real clinical scenario involving hepatic metastases; (3) the evaluation of segmentation results in terms of geometric accuracy and reproducibility; and (4) the demonstration of a reproducible, low-cost, and clinically viable process for 3D printing liver phantoms in resource-limited settings. The remainder of this paper is organized as follows: Section II presents the materials and methods, including the clinical case and segmentation techniques. Section III details the evaluation metrics and results. Section IV discusses the findings in the context of existing literature. Finally, Section V concludes the study and outlines future directions.

II. Materials and Methods

The main steps of the experimental protocol followed in this study are summarized in Fig.1 . Although the steps of 3D modelling, performance evaluation, and comparative analysis are detailed in the Results section, their logical sequence is presented here to provide a structured overall view of the methodology.

A. CT image processing

The computed tomography (CT) images of the liver used in this study were extracted from the open-source Medical Segmentation Decathlon (MSD) database dedicated to liver segmentation. A subset of ten anonymized abdominal volumes was selected from portal venous phase acquisitions, each corresponding to a different patient with various hepatic pathologies, including metastases and hepatocellular carcinoma. These volumes represent a variety of clinical conditions in terms of tumor size, liver morphology, and image quality, making them suitable for evaluating the reproducibility and robustness of segmentation techniques.

The CT scans were acquired using standard clinical protocols, with a matrix size of 512×512 pixels, slice thickness and interslice spacing of 1.25 mm, a tube voltage of 120 kVp, and a current of 35 mA, resulting in high-resolution volumetric data. The acquisition time was approximately 3 minutes and 45 seconds. All datasets were provided in DICOM format, preserving the essential metadata required for accurate medical image analysis. Before segmentation, all CT volumes were visually inspected, and manual reorientation was performed when necessary to ensure spatial consistency and homogeneous preprocessing across the dataset. These steps were crucial to standardize the input data before applying the different segmentation methods evaluated in this study.

B. Clinical Dataset and Case Selection

Ten cases were carefully selected from the CT volumes described. Each case corresponds to a different adult patient presenting with hepatic tumors, mainly metastases or hepatocellular carcinoma, conditions commonly encountered in preoperative planning for liver surgery. Selection was based on:
1. Inclusion criteria: clear visibility of hepatic lesions in

Manuscript received June 8, 2025; Revised August 20, 2025; Accepted August 30, 2025; date of publication September 1, 2025
Digital Object Identifier (**DOI**): https://doi.org/10.35882/jeeemi.v7i4.1086

the portal venous phase; full liver coverage; sufficient image quality to allow accurate segmentation; 2. Exclusion criteria: major motion or reconstruction artifacts, incomplete liver volume, or low-contrast enhancement impairing tumor boundary detection.

Two independent observers validated the final set of cases through visual inspection. This selection aimed to capture a diverse range of tumor sizes, anatomical locations, and liver morphologies, thereby ensuring the clinical applicability and external validity of the segmentation performance evaluation.

C. Segmentation

Segmentation is a crucial process for extracting anatomical components from volumetric medical pictures, especially in 3D modelling for preoperative surgery. This section outlines and contrasts various liver segmentation techniques applied to CT data, including an automatic method (VCAR, GE Healthcare), semi-automatic methods (region growing, thresholding, and contour interpolation) executed with the open-source software 3D Slicer, and a manual segmentation that serves as a reference standard.

1. Automatic Segmentation

The CT volumes from the open-source Medical Segmentation Decathlon database were imported into the proprietary software Hepatic VCAR (GE Healthcare) for automatic segmentation. This module allows for automatically segmenting the liver, tumors, and intrahepatic vascular structures. However, in the context of this study, only the overall shape of the hepatic volume was considered. The automatically segmented vascular structures were ignored, our objective being to compare the quality of the 3D reconstruction of the hepatic parenchyma for accurate anatomical modelling for surgical planning.

Each CT scan can be represented as a 3D matrix of intensity values $I(x,y,z)$ in Hounsfield Units (HU), Eq. gives each voxel volume (1) [42]:

$$V_{voxel} = \Delta_x \cdot \Delta_y \cdot \Delta_z \quad (1)$$

and the segmented liver volume is computed as Eq. (2) [43]:

$$V_{seg} = N_{voxels} \cdot V_{voxel} \quad (2)$$

where N_{voxels} is the number of voxels belonging to the segmented region.

Segmentation in Hepatic VCAR relies on intensity-based filtering and connectivity analysis. A binary mask S_{thresh} is first generated using thresholding Eq. (3) [44]:

$$S_{thresh}(x,y,z) = \begin{cases} 1, & if\ HU_{min} \le I(x,y,z) \le HU_{max} \\ 0, & otherwise \end{cases} \quad (3)$$

to isolate liver tissue intensities in the portal venous phase. The mask is then refined using a connectivity-based region growing process, Eq. (4) [45]:

$$R_{k+1} = R_k \cup \left\{ q \in N(P) \,\middle|\, |I(q) - u_{R_k}| < T \right\} \quad (4)$$

where $N(p)$ is the neighbourhood of voxel P, u_{R_k} is the mean intensity of the current region, and T is a tolerance threshold. Post-processing steps involve morphological operations such as erosion ($A \ominus B$) and dilation ($A \oplus B$) to smooth boundaries and remove noise, Eq. (5) [46]:

$$A \ominus B = \{z | B_z \subseteq A\}; \qquad A \oplus B = \{z | (B_z \cap A) \neq \emptyset\} \quad (5)$$

Finally, a 3D surface mesh of the hepatic volume is reconstructed using the marching cubes algorithm, which extracts the isosurface Eq. (6) [47]:

$$\{(x,y,z) \in \mathbb{R}^3 | I(x,y,z) = I_{iso}\} \quad (6)$$

and tessellates it into triangular facets for accurate anatomical modelling.

2. Region Growth segmentation (Semi-Automatic)

To identify membership in a particular region, we used the region-growing algorithm available in the 3D Slicer software, which primarily considers voxel intensity. This semi-automatic segmentation method relies on intensity similarity between voxels and an initial seed, within a predefined tolerance. It enables progressive expansion of the segmented region starting from manually defined seed points.

The segmentation process can be mathematically expressed using Eq. (7), as follows [48][45]:

$$R = \{x \in D | |I(x) - I(s)| \le \varepsilon\} \quad (7)$$

where R denotes the growing region, D is the image domain, $I(x)$ is the intensity of a candidate voxel, $I(s)$ is the intensity of the seed voxel, and ϵ is the intensity tolerance threshold.

In our protocol, we manually defined two types of seed regions: one corresponding to the liver, and the other to the background (non-hepatic regions). Once the seeds were placed, the "Grow from seeds" tool was activated. The algorithm then proceeded with an automatic expansion of the regions to be segmented from these areas, considering the spatial proximity and intensity similarity of neighbouring voxels. voxels that satisfied the intensity condition described in Eq. (7). The parameters used include a tolerance of ±20 HU around the seed intensity, with a 3D connectivity of the 26-neighbors type.

3. Thresholding-based segmentation (Semi-Automatic)

We used the 3D Slicer software to segment the liver with an initial intensity threshold range between 70 and 160 Hounsfield Units (HU). This approach allowed for the selection of liver tissue; however, other adjacent structures, such as the spleen, bones, and portions of the small intestine, were also included in the segmented area due to overlapping intensity values.

Manuscript received June 8, 2025; Revised August 20, 2025; Accepted August 30, 2025; date of publication September 1, 2025
Digital Object Identifier (**DOI**): https://doi.org/10.35882/jeeemi.v7i4.1086

To address this, the resulting segment was defined as a mask by selecting it as a "modifiable area", which corresponds to the editable region of the image where further segmentation operations can be refined. This mask served as the base for subsequent segmentation steps, including the definition of additional segments, namely “liver” and “background”, to enable application of the region-growing tool. The thresholding method used in this step segments voxels based on their intensity values within a predefined range. It can be mathematically expressed using Eq. (8), as follows [49]:

$$S(x) = \begin{cases} 1, & si\ T_{min} \le I(x) \le T_{max} \\ 0, & Otherwise \end{cases} \quad (8)$$

where $S(x)$ represents the segmentation mask, I(x) is the intensity of voxel x, and $Tmin,Tmax$ These are the lower and upper intensity thresholds. This technique is implemented in the "Threshold" effect within the Segment Editor module of 3D Slicer.

4. Contour interpolation segmentation (Semi-Automatic)

In this method, the segmentation was performed by manually tracing the liver contours every 10 axial slices of the CT dataset using the 3D Slicer software. We intentionally left at least one unsegmented slice between each annotated slice to enable interpolation.

The "Fill Between Slices" tool, available in the segment Editor module, was then used to generate the missing contours through morphological contour interpolation automatically. This algorithm estimates the intermediate segmentations by analysing shape differences between two manually defined contours and gradually morphing one into the other. A manual review was conducted in cases where interpolation produced inaccurate contours at the liver boundaries, to ensure anatomical consistency before exporting the segmented model. Mathematically, the interpolation of the label S at slice z can be approximated as a linear combination between two annotated slices z1 and z2, as shown in Eq. (9) [50] :

$$S_z = (1-\alpha)\cdot S_{Z1} + \alpha \cdot S_{Z2}, \quad with \quad \alpha = \frac{Z-Z_1}{Z_2-Z_1} \quad (9)$$

where Sz represents the interpolated segmentation at slice z, and $\alpha \in [0,1]$ is the relative distance between the two manually segmented slices. This technique reduces manual effort while maintaining anatomical coherence across the segmented volume.

5. Manuel Segmentation

Manual segmentation of the liver was performed using the 3D Slicer software, which precisely traced the contours of the hepatic parenchyma on all CT slices. The work was carried out in the three orthogonal planes: axial (transverse), sagittal (longitudinal), and coronal (frontal), to ensure an accurate three-dimensional representation of the organ. The intuitive interface of 3D Slicer allows for easy coloring of regions of interest, thus facilitating anatomical delineation even in images with low contrast or complex morphology. Although this method is time-consuming, it is considered a gold standard for evaluating the accuracy of semi-automatic or automatic approaches.

The segmentations were performed by a biomedical engineer with seven years of experience in organ segmentation and surgical planning. All manual segmentations were independently reviewed and validated by a second operator with anatomical expertise to reduce subjectivity and potential bias. Any disagreements were resolved through consensus, ensuring the reliability and consistency of the reference segmentation used for evaluation.

D. Creation of the 3D model

After the segmentation of the liver using different approaches (manual, semi-automatic via 3D Slicer, and automatic via GE Healthcare's Hepatic VCAR), the segmented volumes were converted into three-dimensional models. In 3D Slicer, the "Segmentations" module allowed for the generation of a surface mesh from the segmented structures, while in VCAR, the export of the 3D model was carried out directly through the software interface. All the models were then exported in STL (stereo-lithography) format, a standard format for visualization, surgical simulation, and 3D printing. No smoothing or geometric modification operations were applied to preserve the fidelity of the contours resulting from each segmentation method.

E. Evaluation methods

To quantify the geometric discrepancies between the segmented surfaces and the manual reference, the Euclidean distance was used as the fundamental measure between corresponding points. Per image analysis standards, we provide a set of ten mathematical equations supporting the segmentation and evaluation process, detailed below.

It is defined by Eq. 10 and serves as the basis for calculating several geometric indicators, including the Root Mean Square error (RMS) and the Hausdorff Distance (HD) [51].

$$d(x_i, \hat{x}_i) = \|x_i - \hat{x}_i\|_2 \quad (10)$$

where xi and $\hat{x}_i$ are matched vertices on the segmented and reference surfaces, respectively.

The RMS, defined in Eq. 11, measures the mean of the squared Euclidean distances between the segmented model's surface meshes and the reference, thereby providing a global measure of geometric accuracy [52].

$$RMS = \sqrt{\frac{1}{N}\sum_{i=1}^{N}\|x_i - \hat{x}_i\|^2} \quad (11)$$

where xi and $\hat{x}_i$ corresponding points on the reference and test surfaces, respectively, and N is the total number of matched points. The Hausdorff Distance,

Manuscript received June 8, 2025; Revised August 20, 2025; Accepted August 30, 2025; date of publication September 1, 2025
Digital Object Identifier (**DOI**): https://doi.org/10.35882/jeeemi.v7i4.1086

expressed by Eq. 12, captures the maximum deviation between two surfaces, highlighting the most localized errors [53].

$$HD(A,B) = max\left\{\sup_{a\epsilon A}\inf_{b\epsilon B}\|a-b\|, \sup_{b\epsilon B}\inf_{a\epsilon A}\|b-a\|\right\} \quad (12)$$

where A and B are point sets on the respective surfaces. In parallel, the Standard Deviation (SD), given by Eq. 13, was used to assess the variability of segmented liver volumes across different cases, reflecting each method's internal consistency and precision [54].

$$SD = \sqrt{\frac{1}{N}\sum_{i=1}^{n}(V_i - \bar{V})^2} \quad (13)$$

where Vi is the volume in case i, $\bar{V}$and is the mean volume across all cases.

Complementing these geometric measures, the Dice Similarity Coefficient (DSC), defined by Eq. 14, quantifies the volumetric overlap between the segmented result and the manual reference. Unlike other metrics, Dice is based solely on the intersection of voxel sets and does not involve spatial distances [55].

$$DICE = \frac{2|A\cap B|}{|A|+|B|} \quad (14)$$

where A and B denote the sets of voxels from the method under evaluation and the reference segmentation, respectively.

In addition to volumetric analysis, the external surface of the liver model was estimated from the triangular mesh (STL file) [52]. It was computed by summing the areas of each triangle in the mesh, as described in Eq. 15.

$$A = \sum_{i=1}^{M}\frac{1}{2}\left\|(p_{i,1}-p_{i,0})\times(p_{i,1}-p_{i,0})\right\| \quad (15)$$

where M is the total number of triangles and $p_{i,j}$ are the vertices of the triangle. Furthermore, the internal volume of each liver segment was calculated directly from the voxel data. This was done by multiplying the number of voxels labelled within the segment by the volume of a single voxel, as shown in Eq. 16. This straightforward method ensures accurate volume estimation that is independent of surface reconstruction and is particularly useful for evaluating internal consistency across segmentation methods [56].

$$V = N_v \cdot v_{unit} \quad (16)$$

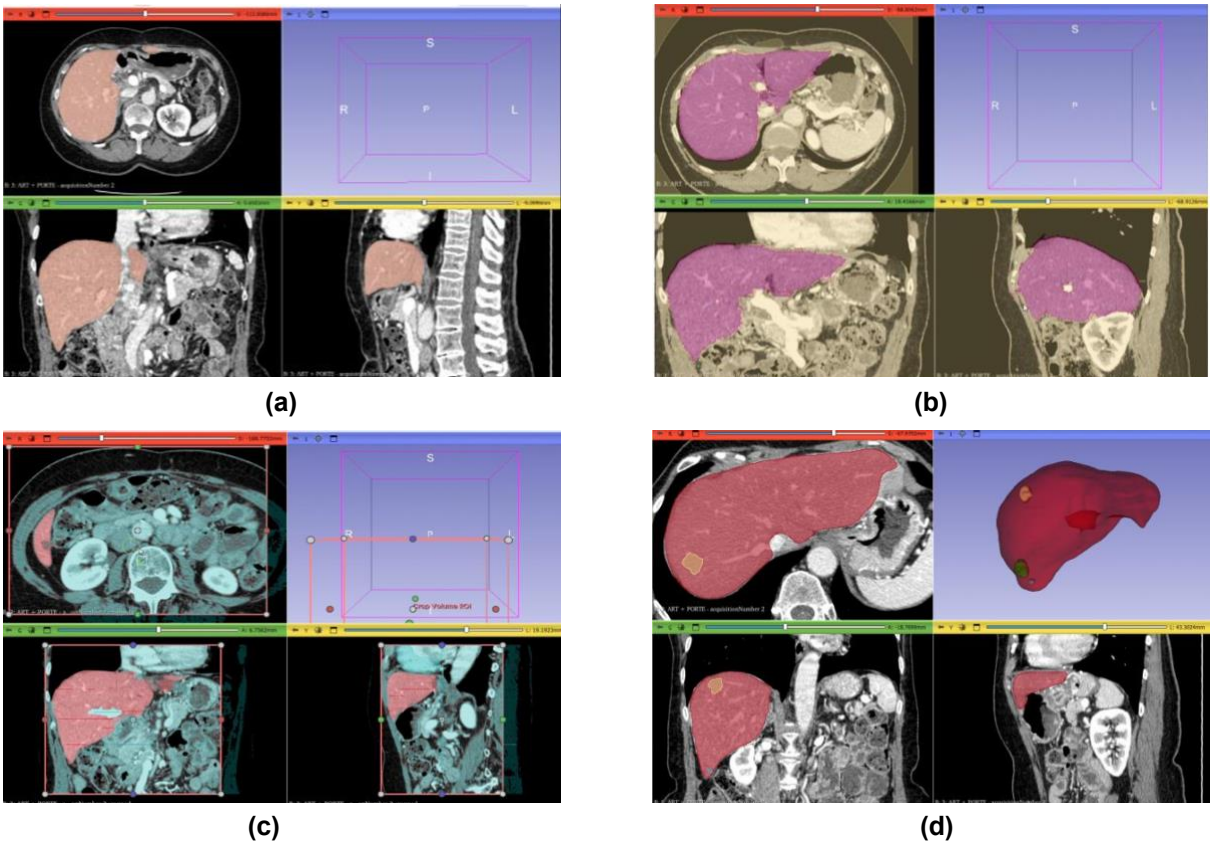

Fig. 2. Segmentation planes axial, sagittal, and coronal. (a) Manual Segmentation; (b) Semi-automatic by regional growth segmentation; (c) Semi-automatic by Thresholding-based segmentation; (d) Semi-automatic by Contour interpolation segmentation.

Manuscript received June 8, 2025; Revised August 20, 2025; Accepted August 30, 2025; date of publication September 1, 2025
Digital Object Identifier (**DOI**): https://doi.org/10.35882/jeeemi.v7i4.1086

Where N_v represents the number of voxels in the segmented region and v_{unit} corresponds to the volume of a single voxel. To evaluate whether the differences in segmentation accuracy between the four tested methods were statistically significant, a non-parametric Friedman test was applied to the RMS, SD, HD, and Dice values, as the data consisted of repeated measures on the same subjects. When the Friedman test revealed significant differences, post hoc pairwise comparisons were performed using the Wilcoxon signed-rank test with Bonferroni correction to control for multiple testing. A significance threshold of $p < 0.05$.

III. Result

The provided data set consists of images in all three planes: axial, sagittal, and coronal. Fig. 2 shows the direction of the three planes used in the data set, including manual and semi-automatic segmentation with 3D Slicer. Fig. 3 shows automatic segmentation with GE Healthcare's Hepatic VCAR. Upon generating each segment for each segmentation method, we transform these segments into three-dimensional forms in STL format for utilization in our simulation. STL files just depict the surface geometry of a three-dimensional object, lacking any color representation. We aligned the liver segmentation models for each method (automatic, semi-automatic by region growing, semi-automatic by thresholding, and semi-automatic by contour interpolation) to compare the distance discrepancies with a manual reference model (ground truth). The alignment of the models allows for an accurate evaluation of the differences between each segmentation method and the ground truth.

The colorimetric mapping of signed deviations between the models is used to visualize these differences. The colors on the models represent the signed deviations: The Red, orange, and yellow areas Indicates significant positive deviations, where the points of the compared model are further away than those of the reference model, The blue zones characterized by negative deviations, where the points of the compared model are closer than those of the reference model, and the green area indicates deviations close to zero within a tolerance of ± 0.2 mm, which means that the points of the two models coincide or are very close (Fig. 4). The bar diagram (Fig. 5) shows deviation (SD) and the Root Mean Square (RMS) for different liver segmentations methods. The precision is determined by applying the standard deviation (SD), which was utilized to measure the dispersion of individual deviations from the average, indicating the internal variability of each method. The Root Mean Square (RMS) quantifies the average of squared deviations, providing a comprehensive measure of accuracy. Together, these two metrics provide a comprehensive assessment of the variability and precision of segmentation methods.

The alignment between the different segmentation methods reveals significant discrepancies in terms of precision and stability. The least reliable alignment is observed with the automatic method, which shows the most excellent dispersion (SD = 2.83 ± 0.20 mm) and the most significant deviations (RMS = 4.64 ± 0.39 mm), indicating a less consistent overall performance. In contrast, the alignment between the semi-automatic method by regional growth and the manual reference shows the lowest dispersion (SD = 0.40 ± 0.12 mm) and the smallest deviations (RMS = 1.48 ± 0.24 mm), making it the most reliable approach among those evaluated. The semi-automatic methods by contour interpolation (SD = 0.99 ± 0.20 mm; RMS = 1.79 ± 0.14 mm) and by

Fig. 3. Segmentation planes, axial, sagittal, and coronal, automatic segmentation with GE Healthcare's Hepatic VCAR.

Manuscript received June 8, 2025; Revised August 20, 2025; Accepted August 30, 2025; date of publication September 1, 2025
Digital Object Identifier (**DOI**): https://doi.org/10.35882/jeeemi.v7i4.1086

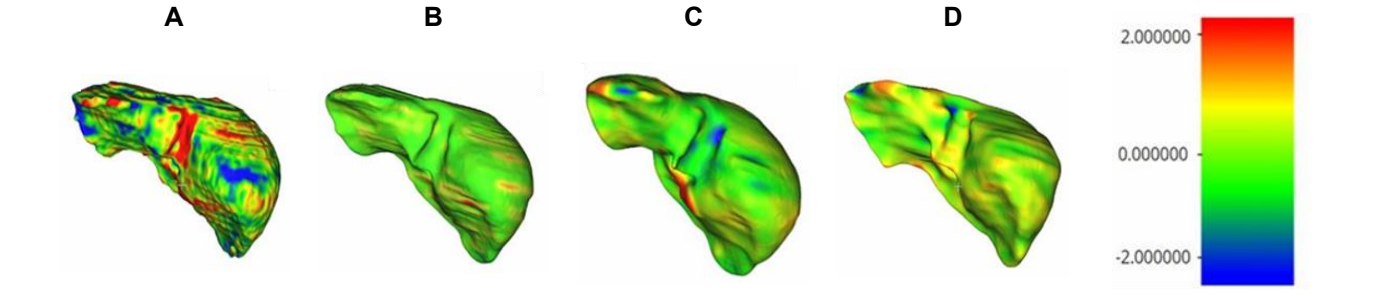

Fig. 4. Colorimetric mapping of significant discrepancies between different models of segmentation of the liver and a manual reference model (ground truth): (A) automatic segmentation; (B) semi-automatic segmentation by region growth; (C) semi-automatic segmentation by thresholding; (D) semi-automatic segmentation by contour interpolation.

thresholding (SD = 1.41 ± 0.25 mm; RMS = 2.03 ± 0.25 mm) show intermediate alignment, with better performance than the automatic method, but inferior to regional growth. These results highlight the importance of good spatial and geometric alignment to ensure precise and reproducible liver segmentation (Fig. 5). The analysis of Root Mean Square (RMS) error and standard deviation (SD) revealed significant differences between segmentation methods (RMS: $p = 2.65 \times 10^{-5}$; SD: $p = 1.38 \times 10^{-6}$). Post hoc Wilcoxon tests ($p < 0.01$) showed that the automatic method was less accurate and more variable than the semi-automatic approaches.

These observations conclude that semi-automatic methods, particularly the region growing approach, exhibit high trueness and precision, consistently producing results that closely match the manual segmentation. The values obtained show strong alignment with the standard reference model. In contrast, the automatic method shows greater variability, reflecting lower trueness and precision, leading to more pronounced discrepancies from the manual reference.

The Dice coefficient (DICE), also known as the overlap index, is the most commonly used metric to validate medical volume segmentations. The semi-automatic segmentation by the region-growing method stands out with the best Dice score (0.935 ± 0.013), reflecting excellent similarity with the reference model. The other semi-automatic methods, contour interpolation and thresholding segmentation, also achieve good scores (0.904 ± 0.016,0.886 ± 0.019), indicating adequate overlap with the reference model. Although the automatic method has the lowest Dice score, with a value of around 0.859 ± 0.025, it still shows good overlap. Overall, all segmentation methods provide

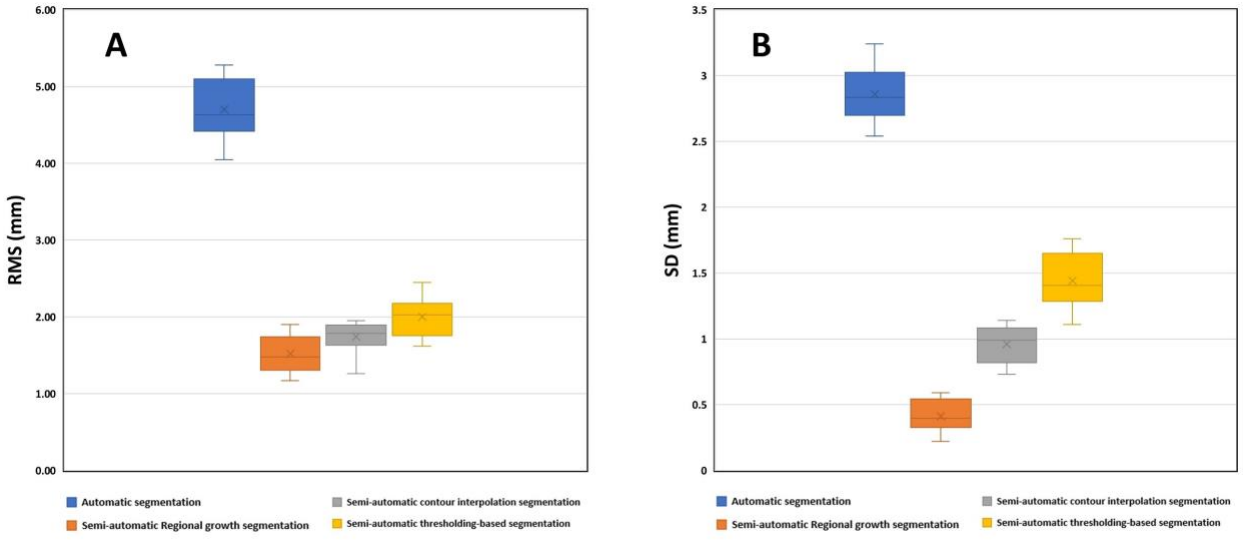

Fig. 5. Boxplots of (a) the precision (SD), and (b) the trueness (RMS) of surface matching between different liver segmentation methods and manual segmentation.

Manuscript received June 8, 2025; Revised August 20, 2025; Accepted August 30, 2025; date of publication September 1, 2025
Digital Object Identifier (**DOI**): https://doi.org/10.35882/jeeemi.v7i4.1086

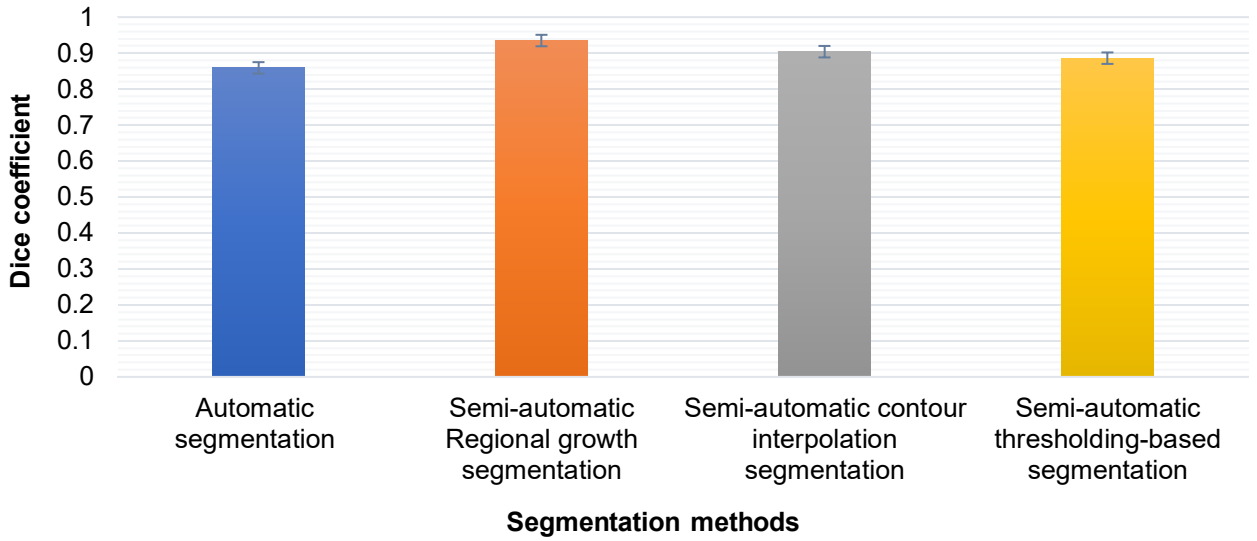

Fig. 6. Comparison of Dice coefficient across different liver segmentation methods.

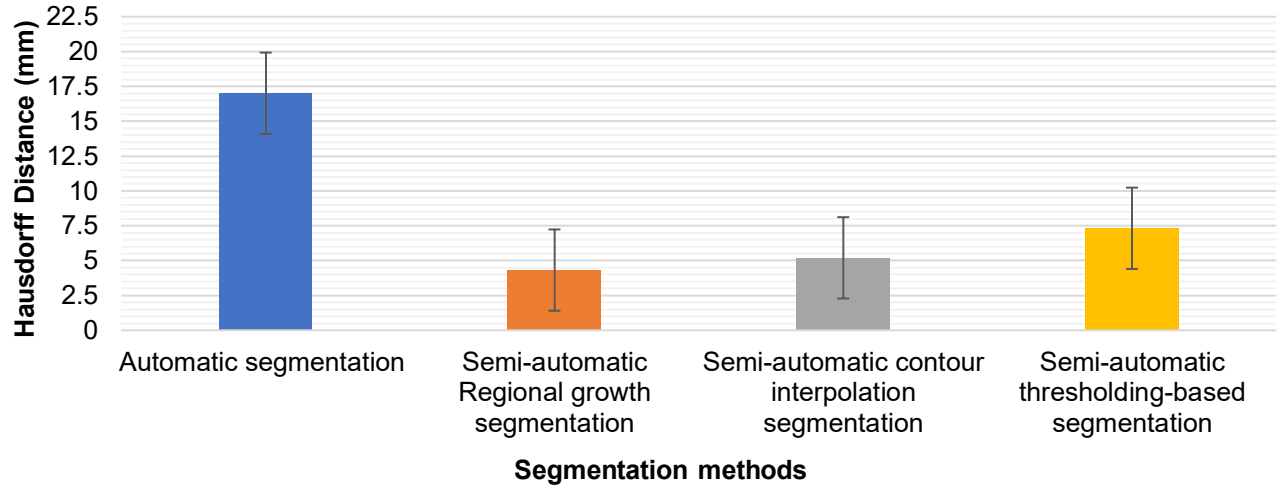

Fig. 7. Comparison of Hausdorff distance across different liver segmentation methods.

satisfactory results regarding overlap with the reference model (Fig. 6).

The Dice coefficient showed significant differences between methods ($p = 3.53 \times 10^{-5}$). The automatic method performed significantly worse than the semi-automatic approaches, particularly the region growing method, which achieved the highest scores and greatest consistency ($p < 0.01$).

Spatial distance-based metrics are widely used in image segmentation evaluation as dissimilarity measures. They are recommended when the overall accuracy of the segmentation. In our case, the Hausdorff distance represents the spatial distance between two sets of points.

The semi-automatic method by region growing shows the lowest Hausdorff distance (4.32 ± 0.48), indicating excellent contour precision. The semi-automatic methods by contour interpolation and thresholding have moderate Hausdorff distances (5.2 ± 0.52,7.32 ± 0.30), respectively, reflecting an acceptable but lower precision than that of region growing. The automatic method displays the highest Hausdorff distance (17.01 ± 1.09), revealing significant inaccuracies in the segmented contours (Fig. 7).

The Hausdorff Distance revealed significant differences between methods ($p = 2.33 \times 10^{-6}$). The automatic method showed the highest local errors, while the region growing approach achieved the lowest HD

Manuscript received June 8, 2025; Revised August 20, 2025; Accepted August 30, 2025; date of publication September 1, 2025
Digital Object Identifier (**DOI**): https://doi.org/10.35882/jeeemi.v7i4.1086

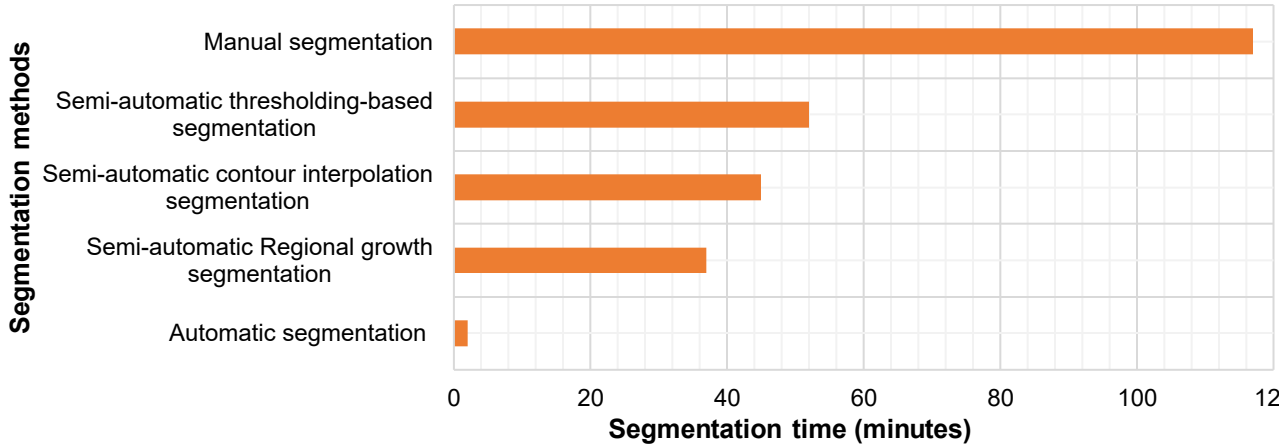

Fig. 8. Comparison of Segmentation Time across Different Methods.

values, confirming its superior geometric accuracy ($p < 0.01$). The time required for liver segmentation varies depending on the method used: region growing, thresholding, contour interpolation, or automatic segmentation. The results demonstrate the superior speed of the automatic method compared to manual or semi-automatic approaches, highlighting the advantages of automation in this type of procedure Fig. 8.

IV. Discussion

This study aimed to evaluate and compare several volumetric liver segmentation methods from CT images, to produce 3D models suitable for surgical planning. The results obtained show that the semi-automatic method using region growing, integrated into the open-source software 3D Slicer, provides the highest performance in terms of geometric fidelity, with a Dice coefficient of 0.935 ± 0.013 and a Hausdorff distance of 4.32 ± 0.48 mm.

The Hausdorff Distance (HD) measures the maximum local deviation between a segmentation and the reference anatomy. Clinically, it indicates worst-case errors, especially near critical structures. An HD below 5 mm is generally required to ensure the reliability of 3D models for surgical planning, as confirmed by Meixner et al. [57] and Konuthula et al.[58], who demonstrated that this threshold guarantees the clinical relevance of anatomical models. These results reflect an excellent match between the segmented contours and the ground truth, with significant inter-case stability as demonstrated by the low dispersion of deviations (SD = 0.40 ± 0.12 mm).

However, despite its overall accuracy, the region growing method may still present limitations in certain challenging cases, such as diffuse steatosis, irregular liver contours, or low-contrast CT scans. These conditions can lead to under- or over-segmentation, especially at the periphery. Such cases highlight the method's sensitivity to anatomical variability and image quality, underscoring the need for visual validation and manual correction to ensure clinical reliability of the 3D models. Regional growth offers significantly superior accuracy compared to other semi-automatic approaches available on the same platform, such as simple thresholding or contour interpolation. Moreover, it substantially surpasses the automatic segmentation provided by the proprietary software Hepatic VCAR, which, although effective in terms of speed, presents less reliable results, notably a lower Dice coefficient (0.859 ± 0.025) and a much higher Hausdorff distance (17.01 ± 1.09 mm), indicating significant discrepancies with the manual reference.

The high standard deviation observed with VCAR indicates significant inter-patient variability, highlighting a lack of robustness that limits its clinical reliability. In contrast, the region growing method shows better adaptability to anatomical variability, especially in complex cases or low-quality CT scans, making it more suitable for clinical use. The region-growing approach, integrated into a free platform such as 3D Slicer, constitutes an immediately applicable solution in resource-constrained clinical environments, consistent with the findings of Cai et al. [31] and Yamaguchi et al. [32], who emphasized the value of semi-automatic methods as a viable alternative to proprietary solutions.

Beyond geometric accuracy, inter-operator reproducibility is crucial for clinical adoption. A preliminary analysis involving two operators on five cases each showed a mean RMS difference of only 0.23 mm with region growing, confirming high consistency when a standard protocol is followed. While the method requires manual input (seed placement and thresholding), its learning curve remains moderate, and reproducible results can be achieved even by non-expert users. This balance

Manuscript received June 8, 2025; Revised August 20, 2025; Accepted August 30, 2025; date of publication September 1, 2025
Digital Object Identifier (**DOI**): https://doi.org/10.35882/jeeemi.v7i4.1086

between precision and usability supports its deployment in resource-limited settings. The creation of realistic and personalized 3D models represents a significant asset for surgical preparation and training, as demonstrated by Rossi et al. [7] and Valls-Esteve et al. [10], who have shown that printed models enhance anatomical understanding and reduce the risk of intraoperative errors.

Unlike VCAR, which lacks manual correction options and shows reduced performance in atypical anatomies, region growing maintains high segmentation quality with a Dice coefficient of 0.935 ± 0.013, RMS of 1.48 mm, and HD of 4.32 mm values well within clinically acceptable thresholds (Dice ≥ 0.90, RMS ≤ 2 mm, HD ≤ 5 mm) [57][59][60][61]. These findings confirm that segmentation quality directly influences the fidelity and clinical relevance of printed models, as reported in studies on the accuracy of medical 3D printing in reconstructive surgery (Juergensen et al. [60]; Chae et al. [61]). Colorimetric deviation maps confirmed that most surface errors in region growing remained under 2 mm, whereas other methods, such as thresholding, contour interpolation, or VCAR, showed more frequent and larger deviations.

Such geometric inaccuracies, if uncorrected, can impact surgical planning by misrepresenting resection margins or vascular landmarks and reduce model usefulness in education. Region growing provides the best trade-off between accuracy, consistency, and flexibility for producing reliable 3D models in line with other studies that demonstrated the robustness and reproducibility of semi-automatic open-source tools such as 3D Slicer in different clinical contexts (Egger et al. [28]; Wijnen et al. [59]).

The performances observed in this study are comparable, if not superior, to those reported in other works using semi-automatic or automatic methods. Yamaguchi et al. [32] developed a semi-automatic method based on a probabilistic atlas and local histograms, achieving a Dice coefficient of 0.912 and a Hausdorff distance of approximately 5.2 mm, slightly lower than our method in terms of accuracy. It is not implemented in a standard open-source platform such as 3D Slicer, which limits its reproducibility and adoption in clinical practice. In contrast, the regional growth method used in our study relies on already available tools, freely accessible, and can be activated without programming or algorithm development, making it an immediately exploitable solution in a real hospital environment. For their part, Cai et al. [31] compared several tools, including a commercial semi-automatic method, and reported a Dice of 0.875 and an RMS of 2.4 mm, which is significantly less precise than the regional growth used in our protocol. More recently, AI-based extensions such as FastSAM-3DSlicer [38] or TomoSAM have been proposed, achieving Dice scores close to 90%. Still, these approaches require specific training, heavy technical infrastructure (GPU), and suffer from algorithmic opacity, which limits their integration into a controlled clinical workflow.

Other studies, such as that of Rundo et al. [62] on using U-Net convolutional neural networks for prostate segmentation, have highlighted similar limitations: although effective in experimental contexts, these models show a strong sensitivity to acquisition variations and artifacts. These limitations, combined with the inability to correct the results manually, restrict their use in surgical practice, especially in resource-limited hospitals. In contrast, our semi-automatic method allows for operator intervention, promoting personalized clinical adaptation without algorithmic retraining.

This study's results align with the work conducted by Egger et al. [28], who validated the robustness and reproducibility of the semi-automatic tools integrated into 3D Slicer in the field of glioblastomas. Although their study subject differs (intracranial structures), their methodology supports using reliable and open semi-automatic solutions in demanding anatomical contexts. Similar approaches have also been validated for liver segmentation within the RVX Liver Segmentation plugin [36], which relies on assisted segmentation but is guided by human expertise.

This combination of precision, accessibility, and flexibility makes our protocol a practical, cost-effective, and immediately applicable solution for surgical teams seeking to integrate 3D modelling into their clinical practice.

A detailed comparison with commercial solutions is needed to fully evaluate the proposed method's clinical applicability, especially in resource-limited settings. Proprietary platforms like Hepatic VCAR or AI-based systems typically require costly licenses, high-performance hardware (e.g., GPUs), and specialized staff, which limits their accessibility in public or under-resourced hospitals.

In contrast, the region-growing method is implemented in 3D Slicer, a free, open-source platform that runs on standard computers and functions offline without requiring cloud access or license fees. Its semi-automatic nature offers transparency and control, enabling clinicians to verify each step. While it requires basic training, even non-experts achieved reproducible results in our study, with a moderate learning curve.

This approach supports efficiently prototyping patient-specific models suitable for preoperative planning and education. Some limitations remain, such as the need for manual adjustments in complex or low-contrast cases and potential onboarding challenges in settings with limited digital expertise. However, the method’s balance of affordability, accessibility,

Manuscript received June 8, 2025; Revised August 20, 2025; Accepted August 30, 2025; date of publication September 1, 2025
Digital Object Identifier (**DOI**): https://doi.org/10.35882/jeeemi.v7i4.1086

adaptability, and precision makes it a strong alternative to commercial systems for sustainable clinical integration.

Although the results obtained are very encouraging, some areas for improvement remain. One of the main upcoming steps concerns the practical validation of the segmented 3D models. Indeed, while the geometric performances have been rigorously quantified using objective metrics (Dice, RMS, HD), these models have not yet been printed or qualitatively evaluated by healthcare professionals in a real surgical setting. Furthermore, one of the main limitations of this study lies in the exclusive reliance on image-derived geometric metrics such as Dice coefficient, Hausdorff Distance, and RMS error for the validation of segmentation accuracy. While these quantitative indicators are essential for assessing spatial agreement with manual references, they do not fully reflect the clinical reality encountered during hepatic resections. The absence of cross-validation against intraoperative findings, resected specimens, or pathological reports limits the direct translatability of the results into clinical decision-making. Indeed, even a segmentation with high geometric scores may fail to capture subtle anatomical variations or tumor margins critical in real-world surgical scenarios. To address this limitation and strengthen clinical relevance, future work should include a validation phase involving comparison with surgical observations and pathology data. For example, correlating segmented volumes with resected tissue measurements, histopathological margins, or navigation data from intraoperative imaging would provide more substantial evidence of the method's applicability in operative contexts. Such validation steps would not only confirm the geometric accuracy but also the anatomical and functional fidelity of the generated 3D models, which is essential for their integration into clinical workflows. Thus, the logical next step in this work will be to materialize the reconstructions in the form of 3D printed physical models, and then submit them to a clinical evaluation by surgeons, radiologists, or anatomists, in order to confirm their anatomical fidelity, pedagogical utility, and added value for surgical planning. Despite the fact that this step is still to be taken, our approach already presents several major advantages. It relies on open-source tools, making it easily deployable in low-resource hospital environments. It does not require advanced IT infrastructure or specific algorithmic expertise, while allowing human intervention at every stage, ensuring clinical control of the outcome. Moreover, it provides high reproducibility, great methodological transparency, and adaptability to complex clinical cases, often poorly handled by automated tools. The printing and future validation of liver models will constitute an additional advancement to strengthen the impact of this method in real-world surgical planning and training contexts. The main objective of this study is to comparatively evaluate several volumetric liver segmentation methods available in open-source software, particularly 3D Slicer, to identify the one offering the best compromise between accuracy, reproducibility, and accessibility, in the context of preoperative 3D modelling. This approach is part of a desire to provide a concrete decision-making tool to practitioners working in resource-limited settings. Continuing this work, a future perspective will involve physically printing the 3D liver models generated from the different segmentation methods, to allow for qualitative evaluation by healthcare professionals (surgeons, radiologists, pathologists). This step will aim to validate the models' anatomical fidelity and clinical relevance in a real surgical planning workflow, thereby enhancing the applied value of the proposed protocol.

V. Conclusion

This study evaluated and compared several liver segmentation methods for 3D surgical planning using open-source tools, particularly 3D Slicer, and found that the semi-automatic method based on region growing demonstrated the best performance, with a Dice similarity coefficient of 0.935 ± 0.013 and a Hausdorff distance of 4.32 ± 0.48 mm, indicating excellent geometric fidelity and strong agreement with manual segmentation. It offered the most favorable balance between precision, reproducibility, and ease of use, particularly in clinical settings with limited resources. An additional finding was that semi-automatic tools allow operator control and correction, leading to more reliable results than fully automatic methods, which are resource-intensive and sensitive to image quality. The use of open-source software further supports accessibility and adaptability in constrained healthcare environments. This study proposes a reproducible and cost-effective workflow for liver segmentation validated using standardized metrics and publicly available CT data, though it lacks physical validation of the 3D models. Future work will involve 3D printing the liver models and assessing them by clinicians to evaluate anatomical fidelity and clinical relevance, thereby enhancing their integration into real-world surgical planning.

Acknowledgment

The authors would like to thank the organizers of the *Medical Segmentation Decathlon* challenge for providing open-access liver CT datasets, which were essential for this study. We also acknowledge the Energy-Materials-Instrumentation and Telecom (EMIT) Laboratory, Faculty of Science and Technology,

Manuscript received June 8, 2025; Revised August 20, 2025; Accepted August 30, 2025; date of publication September 1, 2025
Digital Object Identifier (**DOI**): https://doi.org/10.35882/jeeemi.v7i4.1086

University Hassan 1st, Settat, Morocco, for providing the computational resources used in image processing and 3D reconstruction. Finally, we express our gratitude to colleagues and collaborators for their valuable feedback and constructive discussions during the preparation of this manuscript.

Funding

This research received no specific grant from any funding agency in the public, commercial, or not-for-profit sectors.

Data Availability

The datasets used and analyzed during the current study are available in the Medical Segmentation Decathlon repository, at https://doi.org/10.1038/s41467-022-30695-9.

Author Contribution

LABAKOUM and LYAZIDI conceptualized and designed the study. FARHAN and EL MALALI wrote the initial manuscript. FARHAN, LABAKOUM and MOUHSEN prepared all the figures. All authors reviewed the manuscript, commented on previous versions, and read and approved the final manuscript.

Declarations

Ethical Approval

Not applicable.

Consent for Publication Participants.

All participants gave consent for publication

Competing Interests

The authors declare no competing interests.

References

[1] J. M. Llovet, R. K. Kelley, A. G. Villanueva, A. G. Singal, E. Pikarsky, S. Roayaie, R. Lencioni, K. Koike, Zucman-Rossi, and R. S. Finn, "Hepatocellular carcinoma",Nature Reviews Disease Primers, vol.7", "1

[2] N. Varghese, A. Majeed, S. Nyalakonda, T. Boortalary, D. Halegoua-DeMarzio, and H. Hann, "Review of Related Factors for Persistent Risk of Hepatitis B Virus-Associated Hepatocellular Carcinoma",Cancers, vol.16", "4

[3] A. Nazir, M. Aqib, and M. Usman, "Etiology, Mechanism and Treatment of Liver Cancer",Liver Cancer - Genesis, Progression and Metastasis

[4] H. Maki and K. Hasegawa", Advances in the surgical treatment of liver cancer",BioScience Trends, vol.16, pp.178–188", "3

[5] J.Zhou, H. Sun, Z. Wang, W. Cong, M. Zeng, W. Zhou, P. Bie, L. Liu, T. Wen, M. Kuang, G. Han, Z. Yan, M. Wang, R. Liu, L. Lu, Z. Ren, Z. Zeng, P. Liang, C. Liang, M. Chen, F. Yan, W. Wang, J. Hou, Y. Ji, J. Yun, X. Bai, D. Cai, W. Chen, Y. Chen, W. Cheng, S. Cheng, C. Dai, W. Guo, Y. Guo, B. Hua, X. Huang, W. Jia, Q. Li, T. Li, X. Li, Y. Li, Y. Li, J. T. Liang, C. Ling, T. Liu, X. Liu, S. Lu, G. Lv, Y. Mao, Z. Meng, T. Peng, W. Ren, H. Shi, G. Shi, M. Shi, T. Song, K. Tao, J. Wang, K. Wang, L. Wang, W. Wang, X. Wang, Z. Wang, B. Xiang, B. Xing, J. Xu, Y. Yang, Y. Yang, S. Yang, Z. Yang, S. Ye, Z. Yin, Y. Zeng, B. Zhang, B. Zhang, L. Zhang, S. Zhang, T. Zhang, Y. Zhang, M. Zhao, Y. Zhao, H. Zheng, L. Zhou, J. Zhu, K. Zhu, R. Liu, Y. Shi, Y. Xiao, L. Zhang, C. Yang, Z. Wu, Z. Dai, M. Chen, J. Cai, W. Wang, X. Cai, Q. Li, F. Shen, S. Qin, G. Teng, J. Dong, and J. Fan, "Guidelines for the Diagnosis and Treatment of Primary Liver Cancer (2022 Edition)",Liver Cancer, vol.12, pp.405–444", "5

[6] K. Damiris, H. Abbad, "Cellular based treatment modalities for unresectable hepatocellular carcinoma",World Journal of Clinical Oncology

[7] T. Rossi, A. Williams, and Z. Sun, "Three-Dimensional Printed Liver Models for Surgical Planning and Intraoperative Guidance of Liver Cancer Resection: A Systematic Review",Applied Sciences (Switzerland), vol.13", "19

[8] G. Chen, X. Li, G. Wu, Wang, B. Fang, X. Xiong, R. Yang, L. Tan, S. Zhang, and J. Dong, "The use of virtual reality for the functional simulation of hepatic tumors (case control study)",International Journal of Surgery, vol.8, pp.72–78", "1

[9] S. J. Wigmore, D. N. Redhead, X. J. Yan, J. Casey, K. Madhavan, C. H. C. Dejong, E. J. Currie, and O. J. Garden, "Virtual hepatic resection using three-dimensional reconstruction of helical computed tomography angioportograms",Annals of Surgery, vol.233, pp.221–226", "2

[10] A. Valls-Esteve, A. Tejo-Otero, P. Lustig-Gainza, I. Buj-Corral, F. Fenollosa-Artés, J. Rubio-Palau, I. Barber-Martinez de la Torre, J. Munuera, C. Fondevila, and L. Krauel, "Patient-Specific 3D Printed Soft Models for Liver Surgical Planning and Hands-On Training",Gels, vol.9", "4

[11] Y. Ye, H. Wang, J. Gao, and E. Kostallari, "Editorial: Chronic Liver Disease: New Targets and New Mechanisms",Frontiers in Molecular Biosciences, vol.9

[12] C. E. Mawyin-Muñoz, F. J. Salmerón-Escobar, and J. A. Hidalgo-Acosta, "From Virtual Patients to AI-Powered Training: The Evolution of Medical Simulation",Bionatura Journal, vol.1, pp.1–12", "4

Manuscript received June 8, 2025; Revised August 20, 2025; Accepted August 30, 2025; date of publication September 1, 2025
Digital Object Identifier (**DOI**): https://doi.org/10.35882/jeeemi.v7i4.1086

[13] L. Bresler, M. Perez, J. Hubert, J.P. Henry, and C. Perrenot, "Residency training in robotic surgery: The role of simulation",Journal of Visceral Surgery, vol.157, pp.S123–S129", "3

[14] P. Y. Ng, E. C. Bing, A. Cuevas, A. Aggarwal, B. Chi, S. Sundar, M. Mwanahamuntu, M. Mutebi, R. Sullivan, and G. Parham, "Virtual reality and surgical oncology",Ecancermedicalscience, vol.17, pp.1–15

[15] M. Laspro, L. Groysman, A. V. Verzella, L. Kimberly, and R. Flores, "The Use of Virtual Reality in Surgical Training: Implications for Education, Patient Safety, and Global Health Equity",Surgeries (Switzerland), vol.4, pp.635–646", "4

[16] T. Mori, K. Ikeda, N. Takeshita, K. Teramura, and M. Ito, "Validation of a novel virtual reality simulation system with the focus on training for surgical dissection during laparoscopic sigmoid colectomy",BMC Surgery, vol.22, pp.1–8", "1

[17] R. D. Jacinda, N. P. Yossy, M. D. Kurniatie, I. Hawari, A. W. Setiawan, P. Adidharma, M. Prasetya, M. I. Desem, and T. Asmaria, "Modelling of Human Cerebral Blood Vessels for Improved Surgical Training: Image Processing and 3D Printing",Journal of Electronics, Electromedical Engineering, and Medical Informatics, vol.7, pp.142–153", "1

[18] K. Wang, C. Ho, C. Zhang, and B. Wang, "A Review on the 3D Printing of Functional Structures for Medical Phantoms and Regenerated Tissue and Organ Applications",Engineering, vol.3, pp.653–662", "5

[19] S. Manohar, L. Sechopoulos, M. A. Anastasio, L. Maier-Hein, and R. Gupta, "Super phantoms: advanced models for testing medical imaging technologies",Communications Engineering, vol.3, pp.1–6", "1

[20] Z. Zhao, Y. Ma, A. Mushtaq, V. Radhakrishnan, Y. Hu, H. Ren, W. Song, and Z. T. H. Tse, "Engineering functional and anthropomorphic models for surgical training in interventional radiology: A state-of-the-art review",Proceedings of the Institution of Mechanical Engineers, Part H: Journal of Engineering in Medicine, vol.237, pp.3–17", "1

[21] L.E. Carvalho, A.C. Sobieranski, and A. von Wangenheim, "3D Segmentation Algorithms for Computerized Tomographic Imaging: a Systematic Literature Review",Journal of Digital Imaging, vol.31, pp.799–850", "6

[22] S. Palazzo, G. Zambetta, and R. Calbi, "An overview of segmentation techniques for CT and MRI images: Clinical implications and future directions in medical diagnostics",Medical Imaging Process & Technology, vol.7, pp.7227", "1

[23] H. El malali, A. Assir, "Automatic Mammogram image Breast Abnormality Detection and localization based on the combination of k-means and Genetic algorithms methods",International Journal of Advanced Trends in Computer Science and Engineering, vol.9, pp.76–83", "1.5

[24] H. EL malali, A. Assir, M. Harmouchi, A. Mouhsen, "2020 1st International Conference on Innovative Research in Applied Science, Engineering and Technology (IRASET)"

[25] N. Zaitoun and M. J. Aqel, "Survey on Image Segmentation Techniques",Procedia Computer Science, vol.65, pp.797–806

[26] J.P. Cocquerez, S. Philipp, Ph. Bolon, and J.M. Chassery, "Analyse d'images : filtrage et segmentation"

[27] S. Ray and H. Turi, "Determination of Number of Clusters in K-Means Clustering and Application in Colour Image Segmentation"

[28] J. Egger, T. Kapur, A. Fedorov, S. Pieper, J. V. Miller, H. Veeraraghavan, B. Freisleben, A. J. Golby, C. Nimsky, and R. Kikinis, "GBM volumetry using the 3D slicer medical image computing platform",Scientific Reports, vol.3

[29] M. Puesken, B. Buerke, R. Fortkamp, R. Koch, H. Seifarth, Heindel, and J. Weßling, "Liver lesion segmentation in MSCT: Effect of slice thickness on segmentation quality, measurement precision and interobserver variability",RoFo Fortschritte auf dem Gebiet der Rontgenstrahlen und der Bildgebenden Verfahren, vol.183, pp.372–380", "4

[30] Z. Amla, S. Khehra, A. Mathialagan, and E. Lugez, "Review of the Free Research Software for Computer-Assisted Interventions",Journal of Imaging Informatics in Medicine, vol.37, pp.386–401", "1

[31] W. Cai, B. He, Y. Fan, C. Fang, and F. Jia, "Comparison of liver volumetry on contrast-enhanced CT images: One semiautomatic and two automatic approaches",Journal of Applied Clinical Medical Physics, vol.17, pp.118–127", "6

[32] S. Yamaguchi, K. Satake, Y. Yamaji, Y. Chen, and H. T. Tanaka, "Three-dimensional semiautomatic liver segmentation method for non-contrast computed tomography based on a correlation map of locoregional histogram and probabilistic atlas",Computers in Biology and Medicine, vol.55, pp.79–85

Manuscript received June 8, 2025; Revised August 20, 2025; Accepted August 30, 2025; date of publication September 1, 2025
Digital Object Identifier (**DOI**): https://doi.org/10.35882/jeeemi.v7i4.1086

[33] D. C. Le, K. Chinnasarn, J. Chansangrat, N. Keeratibharat, and P. Horkaew, "Semi-automatic liver segmentation based on probabilistic models and anatomical constraints",Scientific Reports, vol.11, pp.1–19", "1

[34] Z. Yang, Y. Zhao, M. Liao, S. Di, and Y. Zeng, "Semi-automatic liver tumor segmentation with adaptive region growing and graph cuts",Biomedical Signal Processing and Control, vol.68, pp.102670", "April

[35] A. Affane, M. A. Chetoui, J. Lamy, G. Lienemann, R. Peron, P. Beaurepaire, G. Dollé, M. Lèbre, B. Magnin, O. Merveille, M. Morvan, P. Ngo, T. Pelletier, H. S. Rositi, S. Salmon, J. Finet, B. Kerautret, N. Passat, and A. Vacavant, "The R-Vessel-X Project"", "2021

[36] Lamy, Pelletier, Lienemann, Magnin, Kerautret, Passat, Finet, and Vacavant"The 3D Slicer RVXLiverSegmentation plug-in for interactive liver anatomy reconstruction from medical images",Journal of Open Source Software, vol.7, pp.3920", "73

[37] F. Semeraro, A. Quintart, S. F. Izquierdo, and J. C. Ferguson, "TomoSAM: A 3D Slicer extension using SAM for tomography segmentation",SoftwareX, vol.31, pp.1–8

[38] Y. Shen, X. Shao, B. I. Romillo, D. Dreizin, and M. Unberath, "FastSAM-3DSlicer: A 3D-Slicer Extension for 3D Volumetric Segment Anything Model with Uncertainty Quantification", vol.1, pp.1–9

[39] M. Bektaş, C. M. Chia, G. L. Burchell, F. Daams, H. J. Bonjer, and D. L. van der Pee, t"Artificial intelligence-aided ultrasound imaging in hepatopancreatobiliary surgery: where are we now?",Surgical Endoscopy, vol.38, pp.4869–4879", "9

[40] A. Essamlali, V. Millot-Maysounabe, M. Chartier, G. Salin, A. Becq, L. Arrivé, M. D. Camus, J. Szewczyk, and I. Claude, "Bile Duct Segmentation Methods Under 3D Slicer Applied to ERCP: Advantages and Disadvantages",International Journal of Biomedical Engineering and Clinical Science, pp.1–12", "X

[41] Z. Shaukat, Q. A. Farooq, S. Tu, C. Xiao, and S. Ali, "A state-of-the-art technique to perform cloud-based semantic segmentation using deep learning 3D U-Net architecture",BMC Bioinformatics, vol.23, pp.1–21", "1

[42] S. Anand and L. Priya, "Digital Image Fundamentals",A Guide for Machine Vision in Quality Control

[43] S. Gerth, J. Claußen, A. Eggert, N. Wörlein, M. Waininger, T. Wittenberg, and N. Uhlmann, "Semiautomated 3D root segmentation and evaluation based on X-ray CT imagery",Plant Phenomics, vol.2021

[44] P. K. Sahoo, S. Soltani, and A. K. C. Wong, "A survey of thresholding techniques",Computer Vision, Graphics and Image Processing, vol.41, pp.233–260", "2

[45] R. Adams and L. Bischof, "Seeded Region Growing",IEEE Transactions on Pattern Analysis and Machine Intelligence, vol.16, pp.641–647", "6

[46] L. Vincent, "Morphological Grayscale Reconstruction in Image Analysis: Applications and Efficient Algorithms",IEEE Transactions on Image Processing, vol.2, pp.176–201", "2

[47] Lorensen and Cline"Marching Cubes: a High Resolution 3D Surface Construction Algorithm.",Computer Graphics (ACM), vol.21, pp.163–169", "4

[48] A. Mehnert and P. Jackway, "An improved seeded region growing algorithm",Pattern Recognition Letters, vol.18, pp.1065–1071", "10

[49] M. Sezgin, "Survey over image thresholding techniques and quantitative performance evaluation",Journal of Electronic Imaging, vol.13, pp.220", "1

[50] A. B. Albu, T. Beugeling, and D. Laurendeau, "A morphology-based approach for interslice interpolation of anatomical slices from volumetric images",IEEE Transactions on Biomedical Engineering, vol.55, pp.2022–2038", "8

[51] S. Molière, D. Hamzaoui, B. Granger, S. Montagne, A. Allera, M. Ezziane, A. Luzurier, R. Quint, M. Kalai, N. Ayache, H. Delingette, and R. Renard-Penna, "Reference standard for the evaluation of automatic segmentation algorithms: Quantification of inter observer variability of manual delineation of prostate contour on MRI",Diagnostic and Interventional Imaging, vol.105, pp.65–73", "2

[52] H. Kaur, N. Kaur, and N. Neeru, "Evolution of multiorgan segmentation techniques from traditional to deep learning in abdominal CT images – A systematic review",Displays, vol.73, pp.102223", "April

[53] O. U. Aydin, A. A. Taha, A. Hilbert, A. A. Khalil, I. Galinovic, B. Fiebach, D. Frey, and V. I. Madai, "Correction: On the usage of average Hausdorff distance for segmentation performance assessment: hidden error when used for ranking (European Radiology Experimental, (2021), 5, 1, (4), 10.1186/s41747-020-00200-2)",European

Manuscript received June 8, 2025; Revised August 20, 2025; Accepted August 30, 2025; date of publication September 1, 2025
Digital Object Identifier (**DOI**): https://doi.org/10.35882/jeeemi.v7i4.1086

Radiology Experimental, vol.6", "1
[54] R. Cárdenes, de R. Luis-García, and M. Bach-Cuadra, "A multidimensional segmentation evaluation for medical image data",Computer Methods and Programs in Biomedicine, vol.96, pp.108–124", "2
[55] K. H. Zou, S. K. Warfield, A. Bharatha, C. M.C. Tempany, R. Kaus, S. J. Haker, W. M. Wells, A. Jolesz, and R. Kikinis, "Statistical Validation of Image Segmentation Quality Based on a Spatial Overlap Index",Academic Radiology, vol.11, pp.178–189", "2
[56] A. A. Taha and A. Hanbury, "Metrics for evaluating 3D medical image segmentation: Analysis, selection, and tool",BMC Medical Imaging, vol.15", "1
[57] E. Meixner, B. Glogauer, S. Klüter, F. Wagner, D. Neugebauer, L. Hoeltgen, L. Dinges, S. Harrabi, J. Liermann, M. Vinsensia, F. Weykamp, P. Hoegen-Saßmannshausen, J. Debus, and J. Hörner-Rieber, "Validation of different automated segmentation models for target volume contouring in postoperative radiotherapy for breast cancer and regional nodal irradiation",Clinical and Translational Radiation Oncology, vol.49, pp.0–6", "June
[58] N. Konuthula, F. A. Perez, A. M. Maga, W. M. Abuzeid, K. Moe, B. Hannaford, and R. A. Bly, "Automated atlas-based segmentation for skull base surgical planning",International Journal of Computer Assisted Radiology and Surgery, vol.16, pp.933–941", "6
[59] N. Wijnen, L. Brouwers, E. G. Jebbink, J. M. M. Heyligers, and M. Bemelman, "Comparison of segmentation software packages for in-hospital 3D print workflow",Journal of Medical Imaging, vol.8", "03
[60] L. Juergensen, R. Rischen, J. Hasselmann, M. Toennemann, A. Pollmanns, G. Gosheger, and M. Schulze, "Insights into geometric deviations of medical 3d-printing: a phantom study utilizing error propagation analysis",3D Printing in Medicine, vol.10", "1
[61] M. P. Chae, R. D. Chung, J. A. Smith, D. J. Hunter-Smith, and W. M. Rozen, "The accuracy of clinical 3D printing in reconstructive surgery: literature review and in vivo validation study",Gland Surgery, vol.10, pp.2293–2303", "7
[62] L. Rundo, C. Han, Y. Nagano, J. Zhang, R. Hataya, C. Militello, A. Tangherloni, M. S. Nobile, C. Ferretti, D. Besozzi, M. C. Gilardi, S. Vitabile, G. Mauri, H. Nakayama, and P. Cazzaniga, "USE-Net: Incorporating Squeeze-and-Excitation blocks into U-Net for prostate zonal segmentation of multi-institutional MRI datasets",Neurocomputing, vol.365, pp.31–43

Author Biography

LABAKOUM BADREDDINE was born on October 22, 1994, in Agadir, Morocco. He is a Ph.D. student and received his master's degree in biomedical engineering: instrumentation and maintenance from the Faculty of Science and Technology Settat in 2017. His research areas include the applications and evaluation of 3D printing in the medical field and biomedical instrumentation. He works at the Laboratory of Energy-Materials-Instrumentation and Telecom (EMIT), Faculty of Sciences and Technology, Hassan 1st University, Morocco. BP: 577, road to Casablanca. Settat, Morocco. He can be contacted at b.labakoum@uhp.ac.ma

Hamid El Malali was born in Errich-Midelt, Morocco. He holds a doctorate in Biomedical Engineering and Instrumentation Laboratory "RMI" in the Science and Technology Faculty, Hassan 1st University, Settat, Morocco. He has a bachelor's in physics from Sidi Mohammed ben Abdellah University, Fes in 1997, and a Master of Science and Technology in Biomedical Engineering and Instrumentation from Hassan 1st University, Settat in 2016. His research interests are computer vision, image processing, machine learning, and artificial intelligence. In 2003, he holds a diploma in computer science from the Regional Pedagogical Center of Fez. He is a physics and medical imaging professor at Hassan First University, Settat Morocco. He can be contacted at email: h.elmalali@uhp.ac.ma.

Amr Farhan is an assistant professor of biomedical engineering. He received the B.S. degree in Electronic Medical Engineering from Abou Bekr Belkaid Tlemcen University, Algeria, in 2011, and the M.S. degree in Biomedical Instrumentation from the same university in 2013. He obtained his Ph.D. degree in Physics and Engineering Science, specializing in Biomedical Engineering, from Hassan First University of Settat, Morocco, in 2025. His research interests include biomedical engineering, signal processing, 3D printing, machine learning, deep learning, and artificial intelligence, and their applications in the

Manuscript received June 8, 2025; Revised August 20, 2025; Accepted August 30, 2025; date of publication September 1, 2025
Digital Object Identifier (**DOI**): https://doi.org/10.35882/jeeemi.v7i4.1086

biomedical field. He can be contacted at a.farhan@uhp.ac.ma

Azeddine Mouhsen was born on July 10, 1967, and has been a professor of Physics at Hassan First University, Morocco, since 1996. He holds a Ph.D. from Bordeaux I University (France) in 1995 and a thesis from Moulay Ismail University, Morocco, in 2001. He specializes in instrumentation and measurements, sensors, applied optics, energy transfer, and radiation-matter interactions. Azeddine Mouhsen has taught physical sensors, chemical sensors, instrumentation, systems technology, digital electronics, and industrial data processing courses. He has published over 45 papers, and he is the co-inventor of one patent. He is the Director of the Laboratory of Energy-Materials-Instrumentation and Telecom (EMIT). He can be contacted at az.mouhsen@gmail.com

Aissam Lyazidi, Professor at the Higher Institute of Health Sciences, Hassan First University of Settat. He has published over 50 papers. He is the educational coordinator of the biomedical instrumentation and maintenance technologist program in the Higher Institute of Health Sciences, Hassan First University of Settat. His research areas include biomedical engineering applied to clinical practice and medical training. He can be contacted at aissam.lyazidi@uhp.ac.ma

Manuscript received June 8, 2025; Revised August 20, 2025; Accepted August 30, 2025; date of publication September 1, 2025
Digital Object Identifier (**DOI**): https://doi.org/10.35882/jeeemi.v7i4.1086